



PAPER



Cite this: *J. Mater. Chem. C*, 2025, **13**, 5180

Achieving ultra-high anisotropy in thermal conductivity of plastic crystals through megapascal pressure *via* hot pressing†

Zhipeng Wu,^{‡a} Mingzhi Fan,^{‡b} Yangjun Qin,^{‡ac} Guangzu Zhang ^{*b} and Nuo Yang ^{*c}

Plastic crystals, owing to their exceptional properties, are gradually finding applications in solid-state refrigeration and ferroelectric fields. However, their inherently low thermal conductivity restricts their utilization in electronic devices. This study demonstrates that applying megapascal pressure *via* hot pressing can enhance the thermal conductivity of plastic crystal films. Most importantly, it induces significant anisotropy in thermal conductivity. Such anisotropy in thermal conductivity is beneficial for specialized thermal management applications, such as directing heat flow paths in electronic devices. In this study, [(CH₃)₄N][FeCl₄] PC films were prepared *via* hot pressing. At a pressure of 16 MPa, the ratio of in-plane to cross-plane thermal conductivity in the film reaches a remarkable 5.5. This is attributed to the preferential orientation along the (002) crystal plane induced by uniaxial pressure, leading to the formation of a layered structure and the creation of a flat and dense film. Furthermore, according to molecular dynamics simulations, the thermal conductivity along the [100] and [010] directions (parallel to the (002) crystal plane) is higher than in other directions. Therefore, significant modulation of anisotropy in thermal conductivity is achieved in [(CH₃)₄N][FeCl₄] films by applying uniaxial hot pressing pressure. This phenomenon has the potential to greatly broaden the application of plastic crystals in the field of flexible electronic devices.

Received 4th July 2024,
Accepted 16th January 2025

DOI: 10.1039/d4tc02835j

rsc.li/materials-c

1. Introduction

With the progress in solid-state refrigeration, plastic crystals (PCs) have emerged as highly promising materials due to the substantial phase transition entropy generated *via* the barocaloric effect.^{1–4} PCs are a unique class of substances that exhibit characteristics between solid and liquid states, composed of rotatable molecules or ions.^{5,6} PCs exhibit outstanding mechanical deformability^{7,8} and hold great promise as solid-state refrigeration materials.^{1,9,10} In the PC systems, there exists a novel class of plastic/ferroelectric crystals that undergo a transition between the plastic crystal phase and the ferroelectric phase with decreasing temperature.¹¹ [(CH₃)₄N][FeCl₄] is a typical plastic/ferroelectric molecular crystal,^{11–13} showcasing multi-axis ferroelectricity and

excellent plastic deformation capabilities. It can manifest ferroelectric polarization switching and significant piezoelectric response in the form of polycrystalline films. Consequently, PCs demonstrate significant research value in both the fields of solid-state refrigeration and ferroelectricity.

However, PCs exhibit ultra-low intrinsic thermal conductivity at room temperature,^{14–17} which is on the order of 0.1 W m^{−1} K^{−1}, restricting its performance. The structure of PCs has a high disorder and the intermolecular forces are weaker than covalent bonding, leading to significant phonon scattering.^{14,18} Additionally, PCs typically possess substantial compressibility or a small volume modulus,¹ resulting in lower phonon group velocities and weaker intermolecular interactions,^{19,20} thereby demonstrating low thermal conductivity. The lower thermal conductivity poses a significant limitation of its performance and restricts its application, especially in electronics.¹⁴ Research indicates that 55% of electronic device failures result from the accumulation of heat leading to excessively high temperatures.²¹ For electronic devices employing PCs, the low thermal conductivity may give rise to thermal hysteresis and could potentially affect their mechanical performance and charge–discharge rates.^{1,3,22} The accumulation of heat may even induce phase transitions in the sample.¹¹ Therefore, modulating the thermal conductivity of PCs is crucial.

^a School of Energy and Power Engineering, Huazhong University of Science and Technology, Wuhan 430074, China

^b School of Integrated Circuits, Huazhong University of Science and Technology, Wuhan 430074, China. E-mail: zhanggz@hust.edu.cn

^c Department of Physics, National University of Defense Technology, Changsha 410073, China. E-mail: nuo@nudt.edu.cn

† Electronic supplementary information (ESI) available. See DOI: <https://doi.org/10.1039/d4tc02835j>

‡ Z. W., M. F. and Y. Q. contributed equally to this work.

To modulate the thermal conductivity of PCs, methods typically involve altering their microstructure, which can enhance material crystallinity and molecular order, and even induce anisotropy in thermal conductivity. For common organic compounds, the methods such as mechanical stretching,²³ electrospinning,²⁴ nanoscale-templating,²⁵ and hot pressing²⁶ can enhance the thermal conductivity and even induce anisotropy, enabling them to meet diverse heat dissipation requirements.^{27,28} Some studies have found through molecular dynamics (MD) simulations that altering the microstructure can enhance the thermal conductivity of organic polymers.^{29–31} By mechanical stretching,³² a thermal conductivity of $62 \text{ W m}^{-1} \text{ K}^{-1}$ for polyethylene films in the in-plane direction was achieved. For organic ferroelectric materials, electric field polarization can increase molecular chain order, thereby enhancing thermal conductivity along the direction of polarization and generating thermal conductivity anisotropy.³³ Other methods, such as applying shear strain³⁴ and electrospinning,³⁵ can also be used to achieve high in-plane thermal conductivity and generate anisotropy. However, these methods typically present certain challenges in experimental implementation.

Due to the excellent mechanical deformability of PCs, the hot pressing method emerges as a straightforward and effective approach for fabricating films and modulating thermal conductivity.^{11,12} Hot pressing is a common method to prepare organic films, which can change the microstructure of the material.²⁶ In polymer composite systems, hot pressing can induce filler orientation,³⁶ enhance in-plane thermal conductivity, and generate anisotropy.^{37,38} For PCs, a pressure field can also modulate their thermal conductivity. Wang *et al.* found that pressure suppresses the rotation of plastic crystal molecules, reduces resonance, and enhances in-plane thermal conductivity by twofold under a pressure of 3500 MPa.³⁹ Li *et al.* observed a 10% enhancement in the thermal conductivity of neopentyl glycol under 200 MPa.⁴⁰ Xiong *et al.* observed that, for α -quartz, the thermal conductivity along the hexagonal direction only doubles under a pressure of 4 GPa. Furthermore, the ratio of thermal conductivity between the hexagonal direction and the basal direction increases from 1.5 to 2.⁴¹ However, these studies present some questions worth exploring, such as whether an increase in in-plane thermal conductivity can be achieved without adding fillers and whether achieving more pronounced anisotropy in thermal conductivity is feasible under lower pressures.

Here, the impact of pressure during hot pressing on the thermal conductivity of PC films is investigated. In this work, $[(\text{CH}_3)_4\text{N}][\text{FeCl}_4]$ films are prepared using the hot pressing method. It is found that under extremely low uniaxial pressure, the films exhibit exceptionally high anisotropy in thermal conductivity, with a significant increase in in-plane thermal conductivity. And the regulatory mechanisms are discussed by both microscopic structural morphology characterization and molecular dynamics simulations.

2. Experimental and simulation section

The preparation procedure for $[(\text{CH}_3)_4\text{N}][\text{FeCl}_4]$ is as follows: a specific quantity of iron(III) chloride hexahydrate is dissolved in

hydrochloric acid and stirred to obtain solution A. Simultaneously, an equimolar amount of tetramethylammonium chloride is dissolved in deionized water and stirred to form solution B. Subsequently, solutions A and B are mixed and thoroughly stirred, resulting in a clear and transparent yellow solution. At 70°C , the solution undergoes rapid evaporation to yield powder samples for powder X-ray diffraction (XRD) testing. If the solution is left undisturbed for approximately 10 days, yellow crystals precipitate from the solution, constituting $[(\text{CH}_3)_4\text{N}][\text{FeCl}_4]$. Next, PC crystal grains are placed on a hot press, heating to 150°C , and maintaining this temperature to prepare PC films. Subsequently, pressure is applied and maintained for 20 minutes. Upon pressure release, a dense $[(\text{CH}_3)_4\text{N}][\text{FeCl}_4]$ film is formed. The films are then subjected to thermal conductivity testing, differential scanning calorimetry (DSC), XRD, scanning electron microscopy (SEM), and infrared temperature testing. Details of sample preparation are shown in ESI I.†

The thermal conductivity of $[(\text{CH}_3)_4\text{N}][\text{FeCl}_4]$ films were measured using the 3-Omega method. Both the in-plane and the cross-plane value of thermal conductivities were obtained, where electrodes of two different widths were employed. Details of measurements are shown in ESI II.†

The sample images and 3-Omega electrode images of $[(\text{CH}_3)_4\text{N}][\text{FeCl}_4]$ are depicted in Fig. 1(a). To confirm that the samples prepared in this study are $[(\text{CH}_3)_4\text{N}][\text{FeCl}_4]$, XRD and differential scanning calorimetry (DSC) tests were conducted on the samples. The XRD results in Fig. 1(b) align with the XRD results of samples prepared by Harada *et al.*¹¹ Furthermore, DSC tests were performed on the thin film samples in this study. As illustrated in Fig. 1(c), phase transitions occurred around 297 K, 309 K, 350 K, and 385 K, consistent with the reported transition points by Harada *et al.* These findings collectively indicate that the samples obtained in this experiment are $[(\text{CH}_3)_4\text{N}][\text{FeCl}_4]$.

The thermal conductivity of PCs was also calculated using MD simulations, which were conducted using LAMMPS software.^{42–44} Employing the universal force field⁴⁵ and the consistent valence force field,⁴⁶ a simulation of cell of 2780 atoms was performed. Then, thermal conductivities in different directions were obtained by equilibrium molecular dynamics. Simulation of different phases of $[(\text{CH}_3)_4\text{N}][\text{FeCl}_4]$, and the phase III structure is shown in Fig. 1(d). Details of simulations are in ESI III.†

3. Results and discussion

The main finding of this study, shown in Fig. 2(a), is that PC films have a high anisotropy in thermal conductivity, after applying a lower pressure ($>8 \text{ MPa}$) *via* hot pressing. For common inorganic materials like α -quartz and organic materials such as pentaerythritol,^{39,41} a pressure at the GPa level is typically required to double the thermal conductivity and induce significant anisotropy in thermal conductivity. However, the pressure applied in this experiment is only at the MPa level. With increasing pressure, the in-plane thermal conductivity of

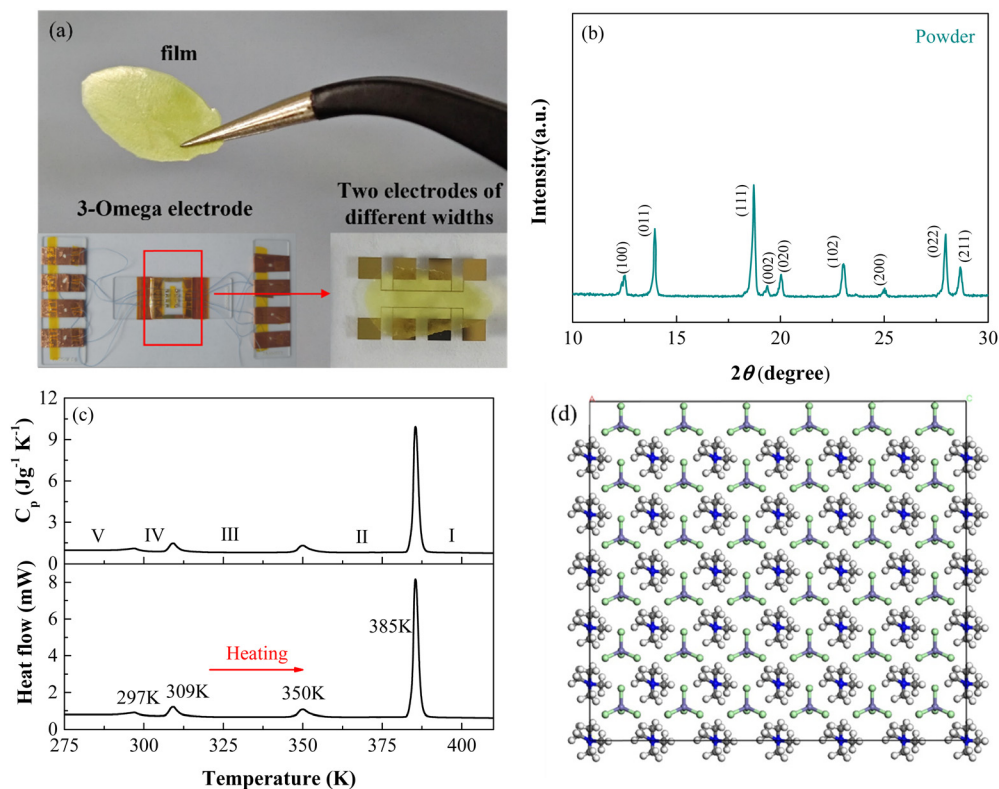


Fig. 1 (a) Film sample and 3-Omega electrode images; (b) XRD pattern of plastic crystals powder; (c) variation of heat capacity and heat flow with temperature in DSC testing; and (d) schematic representation of the phase III structure of $[(\text{CH}_3)_4\text{N}][\text{FeCl}_4]$ molecules.

the sample markedly increases, while the cross-plane thermal conductivity experiences a slight decline. The anisotropic ratio rises from 1.5 to 5.5 corresponding to the pressure increased from 4 to 16 MPa. At a pressure of 16 MPa, the in-plane thermal conductivity of the film reaches $0.59 \pm 0.04 \text{ W m}^{-1} \text{ K}^{-1}$, exhibiting a 146% increase compared to the in-plane thermal conductivity of $0.24 \pm 0.04 \text{ W m}^{-1} \text{ K}^{-1}$ observed at 4 MPa pressure. Moreover, the highest ratio of in-plane to cross-plane thermal conductivity is observed as high as 5.5.

As shown Fig. 2(b), temperature distributions in PC films demonstrate the enhanced thermal conductivity *via* hot pressing pressure. The PC films have dimensions of 6.5 mm in length, and 3.8 mm in width. The cross-sectional area of the films along the X-direction (length) remains constant. The films are placed on a temperature-controlled heating stage, with one end of the film in contact with the heating stage, while the bottom temperatures of both film ends are kept equal (52°C). The other end of the film is exposed to ambient temperature (28°C) without any additional internal heat sources. The convective heat transfer coefficient on the film surface is assumed to be constant, and the emissivity (ε) of the film is set to 0.70. The temperature variation along the x direction in the PC films hot-pressed at 8 MPa is notably smaller. This effect arises because, for rectangular systems with identical cross-sections, higher thermal conductivity leads to reduced thermal resistance along the x direction, resulting in a diminished temperature change along the x direction. Therefore, this further substantiates that pressure indeed enhances the in-plane thermal conductivity of PC films.

Fig. 2(c) shows the change of thermal conductivity of PC films with temperature. The anisotropic ratio of thermal conductivity undergoes a reduction. At room temperature, the samples are the phase III structure of $[(\text{CH}_3)_4\text{N}][\text{FeCl}_4]$,¹¹ which is shown by XRD characterization in Fig. 1(d). There is a phase change when the temperature increases above 350 K.

As shown in the phase III region of Fig. 2(c), the in-plane thermal conductivity exhibits a $T^{-1.3}$ trend. It is similar to the T^{-1} behavior observed in the crystal corresponding to the U process of three phonon scatterings. At elevated temperatures, the phonon vibrations within the lattice become more intense, leading to increased phonon-phonon scatterings, contributing to a noticeable decline in thermal conductivity. Moreover, due to the short-range disordered nature of $[(\text{CH}_3)_4\text{N}][\text{FeCl}_4]$, higher temperatures induce more pronounced molecular rotational motions, diminishing its initial orientational alignment,^{11,47} and consequently reducing the anisotropy.

Besides, Fig. 2(c) shows that the thermal conductivity in the cross-plane direction remains almost unchanged in the phase III. The possible reason is that the presence of numerous grain boundaries along the cross-plane direction limits further changes and phonon scatterings are significant and saturated. And there is little variation with temperature. Therefore, considering both the thermal conductivity along in-plane and cross-plane, the anisotropy in thermal conductivity in the film decreases with increasing temperature.

Moreover, there is obvious change of thermal conductivity when the temperature is above 350 K and the structure changes

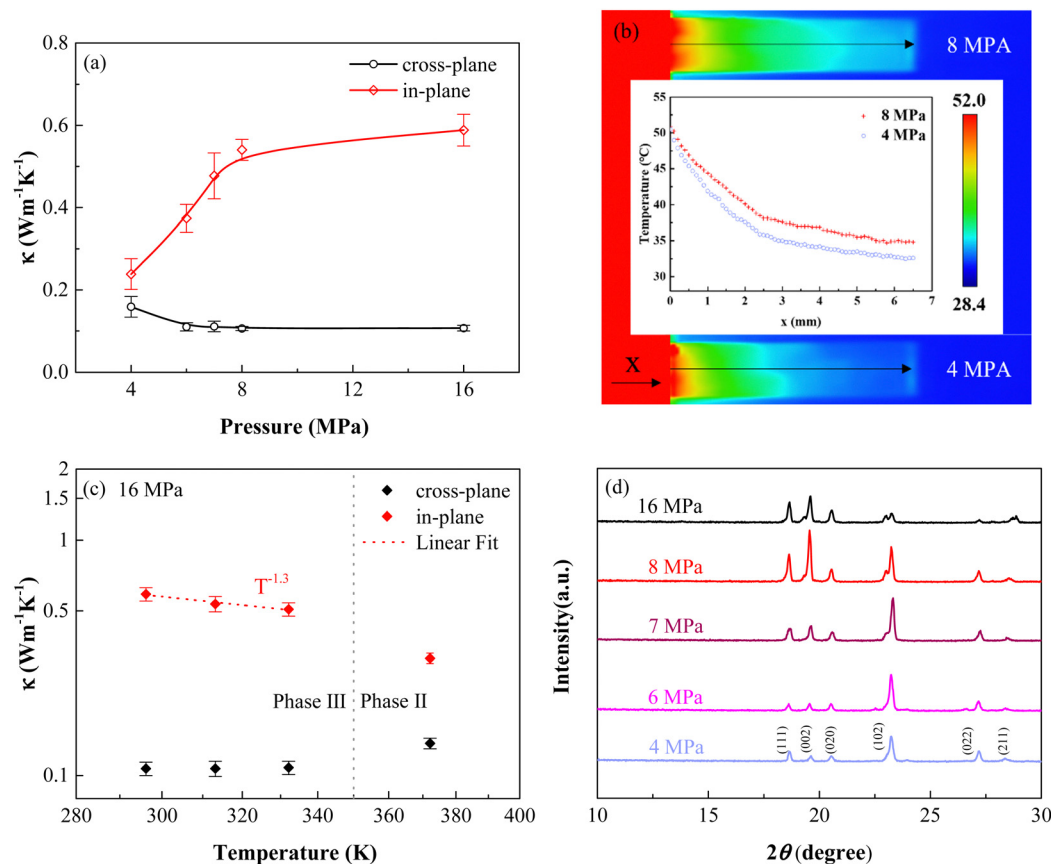


Fig. 2 (a) Variation in thermal conductivity under different pressures (4 MPa, 6 MPa, 7 MPa, 8 MPa, and 16 MPa); (b) infrared thermographs of PC films (8 MPa and 4 MPa) under the same bottom temperature. Inset: Temperature profiles; (c) variation in thermal conductivity under different temperatures; (d) XRD patterns of both plastic crystals powder and films prepared under varying pressures.

to phase II. The fitting line of in-plane data indicates that there is also a trend change in thermal conductivity due to the phase transition. This change is attributed to alterations in the crystal structure and the reorientation of the cations and anions within the structure after the phase transition.

It is worth noting that the property of ultra-high anisotropy in thermal conductivity can greatly expand applications of PCs.^{27,28} The ability to possess ultra-high thermal conductivity along specific planes or directions enhances the suitability of flexible films for specific electronic heat dissipation scenarios, ensuring reliable operating temperatures. Hence, it is essential to investigate the mechanism underlying the anisotropy in thermal conductivity of PC films.

One of the potential reasons for the anisotropy is the preferential orientation of the crystal structure. The XRD patterns of the films are illustrated in Fig. 2(d). It is shown that the intensities of the peaks of (002) and (102) are enhanced with the increasing of pressure. At a hot pressing pressure of 8 MPa, the intensity of the peak of the (002) plane is the highest, indicating a preferential orientation along the (002) crystal plane. This suggests that the application of uniaxial pressure perpendicular to the film surface induces preferential orientation along the (002) crystal plane when large grains undergo deformation or fracture. From the MD simulation results in

Fig. 5, it is evident that the (002) crystal plane exhibits a significantly high thermal conductivity (details will be discussed in the subsequent section on MD simulations). Therefore, orienting along the (002) crystal plane will enhance the thermal conductivity of the PC film and induce anisotropy.

It is worth noting that Harada *et al.* found that for $[(\text{CH}_3)_4\text{N}][\text{FeCl}_4]$ films, the peak of the (002) crystal plane in powder-XRD disappears when the temperature rises to 360 K.¹¹ Additionally, as shown in Fig. 2(c) of this study, when the temperature increases to 372 K, the in-plane thermal conductivity and anisotropy of the film decrease significantly, further demonstrating the important relationship between crystal orientation and anisotropy.

However, when the pressure exceeds 8 MPa, the intensities of the (002) and (102) diffraction peaks markedly decrease. This indicates that excessive pressure partially disrupts the orientation along the (002) and (102) directions, leading to a decrease in thermal conductivity. However, as shown in Fig. 2(a), a slight increase in thermal conductivity is observed. As shown in Fig. 4(d), this is attributed to the pressure-induced formation of distinct layered structures in the film and the formation of nearly single-crystal structures (the details are presented in ESI IV†).

To better elucidate the impact of hot pressing on thermal conductivity, the morphology of the PC films was characterized

by scanning electron microscopy (SEM). The surface morphology of films is shown in Fig. 3. With the increase of pressure, the film surface progressively flattens, and inter-grain bonding improves. At 4 MPa pressure, the film surface exhibits protruding island-like grains. With increasing pressure, the island-like structures diminish, leading to a flatter surface of the film. Gaps between grains are compressed, resulting in closer contact between grains. Consequently, the number of grain boundaries in the in-plane direction decreases, which contributes to enhanced phonon transport in the in-plane direction. Consequently, this results in an increase in the in-plane thermal conductivity of the PC films.

The cross-sectional SEM topography in Fig. 4 offers visual confirmation of the selective crystal orientation and a high anisotropy in thermal conductivity. Fig. 4 illustrates the progressive deformation of grains within the film as pressure increases, leading to the development of a layered structure. At a hot pressing pressure of 4 MPa, the pressure induces a tilted state in part of the grain boundary, and there are still some substantial pores present between grains. Upon increasing the pressure to 6 MPa, laminated grains begin to manifest within the film. Further elevation of pressure to 8 MPa results in robust interconnection of grains along the in-plane direction, accentuating the emergence of a more distinct layered structure. This phenomenon may arise due to the pressure conditions favoring the interconnection of grains along the

in-plane direction, consequently enhancing the thermal transport capacity within the plane. This results in the crystal exhibiting preferential orientation along the (002) crystal plane. It is worth noting that when the pressure reaches 16 MPa, a distinct layered structure appears within the film. This is attributed to the gradual compression of grains into elongated shapes under increasing uniaxial pressure, leading to tight interconnections between grains along the in-plane direction and the formation of a layered structure. The emergence of this layered structure significantly elevates the thermal transport performance in the in-plane direction.

It is noteworthy that, for the cross-plane direction, with increasing pressure, the compression of grains results in a higher number of grain boundaries per unit length. Additionally, the fragmentation of grains generates additional grain boundaries. Therefore, under the influence of pressure, the film gradually forms a layered structure in the cross-plane direction. This inhibits thermal transport along the cross-plane direction, resulting in a reduction in cross-plane thermal conductivity. Therefore, under the influence of hot pressing, the crystals in the PC film undergoes preferential orientation along the in-plane direction, leading to the emergence of a layered structure. This results in a significant anisotropy in the thermal conductivity of the film.

However, at a pressure of 16 MPa, noticeable fractures occur within the layered region, indicating that the thermal conductivity

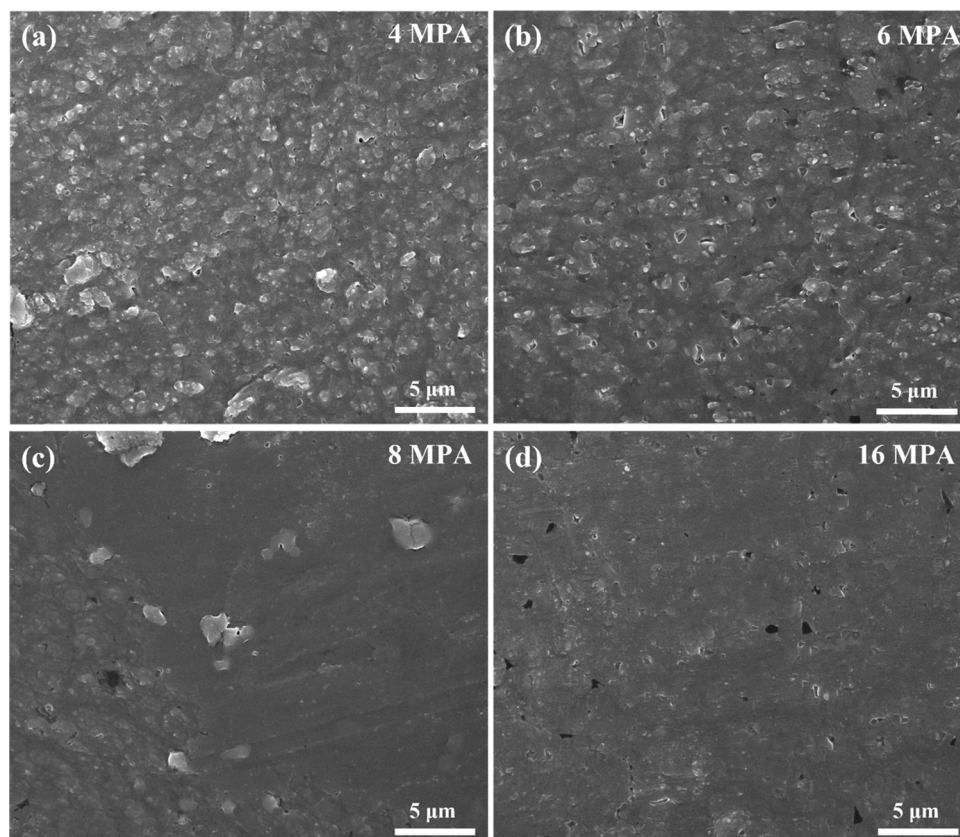


Fig. 3 SEM surface morphology of PC films prepared under varying pressures: (a) 4 GPa, (b) 6 MPa, (c) 8 MPa, and (d) 16 MPa.

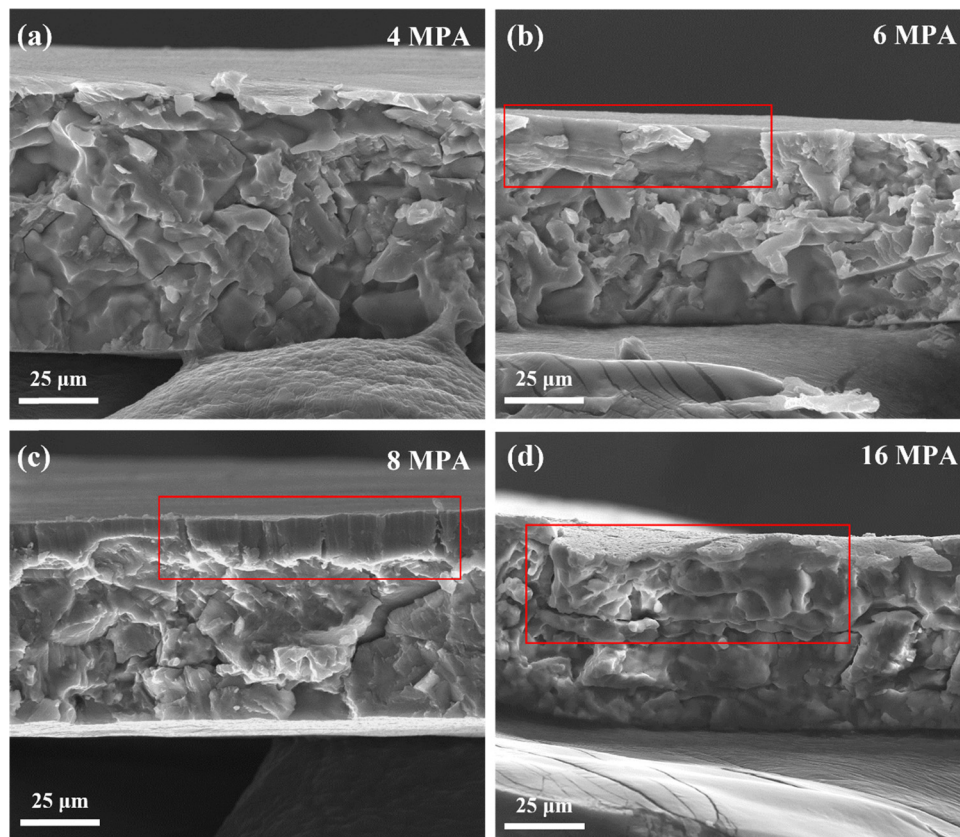


Fig. 4 SEM cross-sectional morphology of PC films under varying pressures: (a) 4 GPa, (b) 6 MPa, (c) 8 MPa, and (d) 16 MPa.

along the in-plane direction becomes constrained when the pressure reaches a certain threshold. Consequently, as depicted in Fig. 2(a), the in-plane thermal conductivity of the film pressed at 16 MPa exhibits virtually no further increase.

As for the impact of density, quantitative measurements reveal that the density of the PC film is changed 4% within the pressure range from 4 to 16 MPa, as shown in Table S1 (ESI†). This can be attributed to the inherent plasticity of $[(\text{CH}_3)_4\text{N}][\text{FeCl}_4]$, which, under uniaxial pressure, causes the crystal to elongate along other directions, resulting in small changes in density. Therefore, density has minimal impact on the thermal conductivity of the PC films in this study.

Furthermore, the change in porosity is relatively small, resulting in a limited impact on thermal conductivity. This is because the density of the film changes only slightly with increasing pressure, leading to minimal variation in porosity. Porous structures contain numerous grain boundaries, and the abundance of these boundaries prevents thermal conductivity from exhibiting anisotropy. As the pressing pressure increases, pores undergo compression and deformation, and the number of boundaries between crystals gradually decreases, leading to the formation of nearly single-crystalline structures. These crystalline structures introduce anisotropy. Moreover, the phonon mean free path in crystalline structures is expected to be much larger than that in porous structures. Therefore, changes in crystal morphology significantly influence thermal conductivity.

To investigate the mechanism behind the changes in thermal conductivity, MD simulations were conducted to explore the thermal conductivity of $[(\text{CH}_3)_4\text{N}][\text{FeCl}_4]$ along a couple of directions (Fig. 5(a)). In calculating the thermal conductivity *via* the equilibrium MD, the heat flow autocorrelation function is integrated. Fig. 5(b) illustrates the trend of thermal conductivity and heat current autocorrelation function (HCACF) with correlation time. To ensure the accuracy of the calculation, the average was taken from 8 cases with different initial conditions. (Details of simulations are given in ESI III†.)

The simulation results reveal that the intrinsic thermal conductivity of at 330 K (phase III) has distinct values along different directions. The highest thermal conductivity is $0.39 \pm 0.09 \text{ W m}^{-1} \text{ K}^{-1}$ along [100] directions, which is close to 7.8 times higher than that along the [011] direction ($0.06 \pm 0.02 \text{ W m}^{-1} \text{ K}^{-1}$). The directions [100] and [010] are parallel to the (002) plane. That is, the (002) plane likely corresponds to the in-plane direction. It coincides with the measured results that the thermal conductivity along the in-plane direction is higher than the cross-plane. Additionally, Fig. 2(a) shows that when the pressure increases to 8 MPa and 16 MPa, the ratio of thermal conductivity between in-plane and cross-plane directions is 5.1 and 5.5, respectively.

In Fig. 5(a), it can be observed that the spread of thermal conductivities in phase II is smaller than in phase III. This indicates that as the temperature increases and the phase

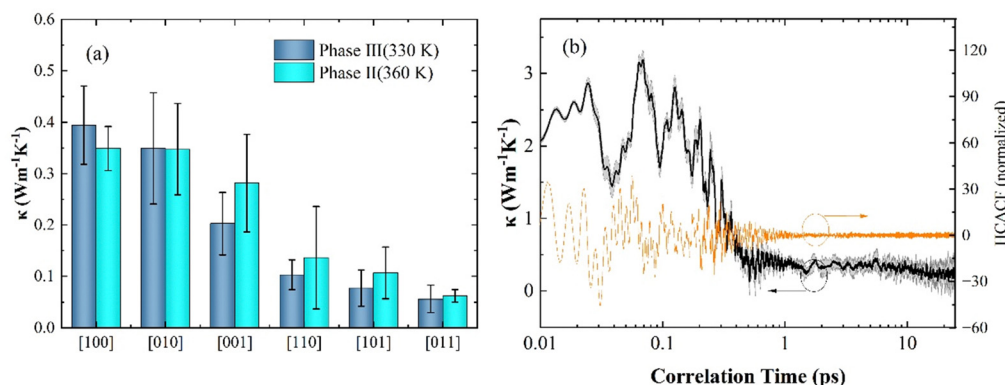


Fig. 5 (a) The values of thermal conductivity of $[(\text{CH}_3)_4\text{N}][\text{FeCl}_4]$ along different directions by MD simulations: values for phase III (corresponding to the temperature spread as $309 \text{ K} < T < 350 \text{ K}$), and phase II ($350 \text{ K} < T < 385 \text{ K}$). (b) The normalized HCACF and the thermal conductivity of PCs as a function of correlation time along the [100] direction at 360 K.

change, the anisotropy in thermal conductivity diminishes, which is also consistent with the experimental results. There are two primary reasons for this phenomenon. Firstly, the number of primitive cell atoms of phase II is 44 which is twice that of phase III (shown in Fig. 6). The increase in atomic density introduces more phonon branches and significantly raises the probability of phonon–phonon scattering. Secondly, phase II corresponds to a higher temperature, which takes anharmonic effects of the phonon vibrations. It also leads to an increase of phonon–phonon scattering and a decrease in thermal conductivity.

One of the possible reasons for the anisotropy is the different atomic coupling force along different directions. In PCs, coulombic forces play a dominant role.⁴⁸ And $[(\text{CH}_3)_4\text{N}][\text{FeCl}_4]$ experiences different coulombic forces along the [100], [010], [001], [110], [101], and [011] directions. For phase III, it was found that the coulombic force constant along the [100] direction ($69 \text{ eV } \text{\AA}^{-1}$) is 5.3 times stronger than that along the [101] and [011] directions ($12.9 \text{ eV } \text{\AA}^{-1}$ and $13.3 \text{ eV } \text{\AA}^{-1}$), which is calculated using MD. Consequently, this result shows significant differences in thermal transport capabilities along different directions.

At 360 K (phase II), the anisotropy in thermal conductivity of $[(\text{CH}_3)_4\text{N}][\text{FeCl}_4]$ diminishes. Compared to phase III, the thermal conductivity at 360 K increases in the [001], [110], [101] and [011] directions, resulting in a reduction in its overall anisotropy. This simulation results coincide with the measured

results in Fig. 2(c), where the discrepancy in intrinsic thermal conductivity values among different directions diminishes with increasing temperature.

The values of thermal conductivity by MD are around 54.2% higher than those by measurements of polycrystalline films. This discrepancy is rational given the inherent differences between the simulated systems and experimental samples. One possible reason is that the polycrystalline samples display the presence of grain boundaries and other defects. These imperfections lead to increased phonon scattering at interfaces, thereby reducing thermal conductivity. Additionally, the measurements were taken in the in-plane direction which includes different crystal directions and may include directions of lower thermal conductivity.

MD simulations were employed to compute the thermal conductivity of single crystals under 0 MPa conditions, yielding results higher than experimental measurements on polycrystalline films, which is a reasonable outcome. However, at 8 MPa and 16 MPa, the experimental values exceeded the results of the simulations. This disparity may stem from the inability of conventional force fields to accurately describe the thermal properties of the system. Furthermore, the lack of suitable potential functions for these ionic crystal plastic crystals has made qualitative studies a focal point in this aspect of molecular simulations.⁴⁹

Therefore, the anisotropic thermal conductivity of the PC material studied here is primarily influenced by the microstructure and orientation of crystal structures.

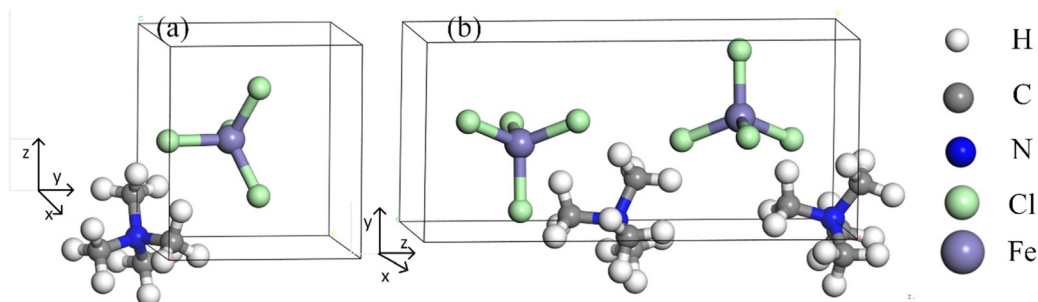


Fig. 6 The structure of primitive cell: (a) phase III, and (b) phase II.

From the SEM cross-sectional image (Fig. 4) and XRD data (Fig. 2(d)), it is evident that the film pressed at 4 MPa exhibits an unordered polycrystalline structure with disordered porous crystals. As the pressure increases, large layered grains gradually form within the film, and the intensity of the (002) crystal plane peak increases. Under 8 MPa hot-pressing, a clear formation of large layered grains is observed in the upper half of film samples.

Under 16 MPa hot-pressing, larger and more distinct single-crystal-like structures emerge within the film, forming pronounced layered structures, as shown in Fig. 4(d) of the main text. Its XRD pattern shows only three main peaks: (002), (111), and (020), with other peaks either disappearing or weakening, also indicating that the film approaches a single-crystal state.

Additionally, the MD simulation results (Fig. 5) show that a perfect single-crystal structure exhibits significant thermal conductivity anisotropy, with the highest thermal conductivity along the [100] and [010] directions (parallel to the (002) crystal plane). Therefore, as the pressure increases, the crystals preferentially orient along the (002) plane, forming more complete layered structures that approach a single-crystal state, leading to an increase in the in-plane thermal conductivity and a significant thermal conductivity anisotropy in the film.

4. Conclusions

In summary, the thin film of the $[(\text{CH}_3)_4\text{N}][\text{FeCl}_4]$ plastic crystal, synthesized through uniaxial pressure hot pressing, demonstrates an ultra-high anisotropy in thermal conductivity at extremely low pressures. Specifically, under an increased pressure of 16 MPa, the in-plane thermal conductivity of the film can reach $0.59 \text{ W m}^{-1} \text{ K}^{-1}$, with an exceptionally high ratio of in-plane to cross-plane thermal conductivity, reaching 5.5. This is attributed to the outstanding mechanical deformability of $[(\text{CH}_3)_4\text{N}][\text{FeCl}_4]$ in its PC phase, which allows it to exhibit a preferred orientation along the (002) crystal plane under uniaxial pressure. This leads to the formation of a layered structure, resulting in a smooth and dense film surface. Additionally, in phase III, the thermal conductivity along the [100] and [010] directions (parallel to the (002) crystal plane) surpasses that along the [001] direction. Consequently, $[(\text{CH}_3)_4\text{N}][\text{FeCl}_4]$, when hot-pressed into a film, exhibits a remarkable anisotropy in thermal conductivity at room temperature. The ability to achieve the substantial regulation of anisotropy in thermal conductivity with minimal pressure holds promise for expanding the applications of PC films in flexible electronic devices and thermal switches.

Author contributions

Zhipeng Wu: investigation, writing – original draft, data curation, formal analysis. Mingzhi Fan: investigation, writing – original draft, data curation. Yangjun Qin: investigation, writing – original draft, software. Guangzu Zhang: project administration, conceptualization, writing – review & editing. Nuo Yang: project administration, conceptualization, writing – review & editing.

Data availability

The data that support the findings of this study are available on request from the corresponding author upon reasonable request.

Conflicts of interest

There are no conflicts of interest to declare.

Acknowledgements

This work was financially supported by the National Natural Science Foundation of China (52172114 and 52372108). The work was carried out at the National Supercomputer Center in Tianjin, and the calculations were performed on the Tianhe new generation supercomputer.

References

- 1 B. Li, Y. Kawakita and S. Ohira-Kawamura, *et al.*, *Nature*, 2019, **567**, 506–510.
- 2 X. Moya, S. Kar-Narayan and N. D. Mathur, *Nat. Mater.*, 2014, **13**, 439–450.
- 3 P. Lloveras, A. Aznar and M. Barrio, *et al.*, *Nat. Commun.*, 2019, **10**, 1803.
- 4 A. Aznar, P. Lloveras and M. Barrio, *et al.*, *J. Mater. Chem. A*, 2020, **8**, 639–647.
- 5 J. L. Tamarit, B. Legendre and J. M. Buisine, *Mol. Cryst. Liq. Cryst.*, 1994, **250**, 347–358.
- 6 R. Brand, P. Lunkenheimer and A. Loidl, *J. Chem. Phys.*, 2002, **116**, 10386–10401.
- 7 J. Harada, T. Shimojo and H. Oyamaguchi, *et al.*, *Nat. Chem.*, 2016, **8**, 946–952.
- 8 H. Zhu, D. R. Macfarlane and J. M. Pringle, *et al.*, *Trends Chem.*, 2019, **1**, 126–140.
- 9 S. Das, A. Mondal and C. M. Reddy, *Chem. Soc. Rev.*, 2020, **49**, 8878–8896.
- 10 K. Zhang, R. Song and J. Qi, *et al.*, *Adv. Funct. Mater.*, 2022, **32**, 2205635.
- 11 J. Harada, N. Yoneyama and S. Yokokura, *et al.*, *J. Am. Chem. Soc.*, 2018, **140**, 346–354.
- 12 J. Harada, Y. Kawamura and Y. Takahashi, *et al.*, *J. Am. Chem. Soc.*, 2019, **141**, 9349–9357.
- 13 J. Harada, *APL Mater.*, 2021, **9**, 20901.
- 14 S. Wang, L. Sun and B. Li, *et al.*, *J. Phys. Chem. C*, 2021, **125**, 15853–15862.
- 15 S. Akbulut, Y. Ocak and K. Keşlioğlu, *et al.*, *J. Phys. Chem. Solids*, 2009, **70**, 72–78.
- 16 D. Li, X. Zhao and H. Zhao, *et al.*, *Inorg. Chem.*, 2019, **58**, 655–662.
- 17 A. Salvatori, D. Aguilà and G. Aromí, *et al.*, *J. Mater. Chem. A*, 2023, **11**, 12140–12150.
- 18 B. Li, Y. Kawakita and Y. Liu, *et al.*, *Nat. Commun.*, 2017, **8**, 16086.

- 19 J. Qi, B. Dong and Z. Zhang, *et al.*, *Nat. Commun.*, 2020, **11**, 5197.
- 20 A. I. Krivchikov, G. A. Vdovichenko and O. A. Korolyuk, *et al.*, *J. Non-Cryst. Solids*, 2015, **407**, 141–148.
- 21 Z. Khattak and H. M. Ali, *Int. J. Heat Mass Transfer*, 2019, **130**, 141–161.
- 22 A. Fallahi, G. Guldentops and M. Tao, *et al.*, *Appl. Therm. Eng.*, 2017, **127**, 1427–1441.
- 23 S. Shen, A. Henry and J. Tong, *et al.*, *Nat. Nanotechnol.*, 2010, **5**, 251–255.
- 24 J. Gu, Z. Lv and Y. Wu, *et al.*, *Composites, Part A*, 2017, **94**, 209–216.
- 25 V. Singh, T. L. Bougher and A. Weathers, *et al.*, *Nat. Nanotechnol.*, 2014, **9**, 384–390.
- 26 W. Liu, Z. Lei and R. Yang, *et al.*, *ACS Appl. Mater. Interfaces*, 2022, **14**, 10605–10615.
- 27 A. L. Moore and L. Shi, *Mater. Today*, 2014, **17**, 163–174.
- 28 C. P. Feng, F. Wei and K. Y. Sun, *et al.*, *Nano-Micro Lett.*, 2022, **14**, 127.
- 29 A. Henry and G. Chen, *Phys. Rev. Lett.*, 2008, **101**, 235502.
- 30 X. Yu, D. Ma and C. Deng, *et al.*, *Chin. Phys. Lett.*, 2021, **38**, 103–116.
- 31 X. Wan, B. Demir and M. An, *et al.*, *Int. J. Heat Mass Transfer*, 2021, **180**, 121821.
- 32 Y. Xu, D. Kraemer and B. Song, *et al.*, *Nat. Commun.*, 2019, **10**, 1771.
- 33 S. Deng, J. Yuan and Y. Lin, *et al.*, *Nano Energy*, 2021, **82**, 105749.
- 34 Z. Li, L. An and S. Khuje, *et al.*, *Sci. Adv.*, 2021, **7**, i7410.
- 35 Z. Chen, S. Gao and J. Zhang, *et al.*, *Compos. Commun.*, 2023, **41**, 101654.
- 36 C. Yu, W. Gong and W. Tian, *et al.*, *Compos. Sci. Technol.*, 2018, **160**, 199–207.
- 37 P. Ding, J. Zhang and N. Song, *et al.*, *Compos. Sci. Technol.*, 2015, **109**, 25–31.
- 38 B. Yao, L. An and H. Zhu, *et al.*, *Energy Convers. Manage.*, 2023, **276**, 116603.
- 39 S. Wang, H. Fan and Z. Zhang, *et al.*, *J. Mater. Chem. C*, 2022, **10**, 14431–14438.
- 40 F. Li, M. Li and C. Niu, *et al.*, *Appl. Phys. Lett.*, 2022, **120**, 73902.
- 41 X. Xiong, E. J. Ragasa and A. Chernatynskiy, *et al.*, *J. Appl. Phys.*, 2019, **126**, 215106.
- 42 Z. Zong, S. Deng and Y. Qin, *et al.*, *Nanoscale*, 2023, **15**, 16472–16479.
- 43 J. Ma, S. Wang and X. Wan, *et al.*, *Nanoscale*, 2022, **14**, 17072–17079.
- 44 A. P. Thompson, H. M. Aktulga and R. Berger, *et al.*, *Comput. Phys. Commun.*, 2022, **271**, 108171.
- 45 A. K. Rappe, C. J. Casewit and K. S. Colwell, *et al.*, *J. Am. Chem. Soc.*, 1992, **114**, 10024–10035.
- 46 P. Dauber-Osguthorpe, V. A. Roberts, D. J. Osguthorpe, J. Wolff, M. Genest and A. T. Hagler, *Proteins: Struct., Funct., Bioinf.*, 1988, **4**(1), 31–47.
- 47 V. A. Konstantinov, V. P. Revyakin and V. V. Sagan, *Low Temp. Phys.*, 2006, **32**, 689–694.
- 48 K. Huang, *Solid State Physics*, Higher Education Press, Beijing, 2005, pp. 49–55.
- 49 Y. Qin, Z. Zong, J. Che, T. Li, H. Fang and N. Yang, *arXiv*, 2025, **2501**, 12078.

Supporting Information

Achieving ultra-high anisotropy in thermal conductivity of plastic crystal through megapascal pressure of hot pressing

Zhipeng Wu^{1, #}, Mingzhi Fan^{2, #}, Yangjun Qin^{1,3, #}, Guangzu Zhang^{2, †}, Nuo Yang^{3, †}

1) School of Energy and Power Engineering, Huazhong University of Science and Technology, Wuhan 430074, China

2) School of Intergrated Circuits, Huazhong University of Science and Technology, Wuhan 430074, China

3) Department of Physics, National University of Defense Technology, Changsha 410073, China

Z. W., M. F. and Y. Q. contributed equally to this work.

†Corresponding E-mail: G.Z. (zhanggz@hust.edu.cn) and N.Y. (nuo@nudt.edu.cn)

SM I. Details of sample preparation

Preparation of $[(\text{CH}_3)_4\text{N}][\text{FeCl}_4]$ involves the following steps. 1.6218 g of iron(III) chloride hexahydrate (AR, Aladdin) is accurately weighed and dissolved in 4 mL hydrochloric acid (AR, Sinopharm), resulting in solution A after 30 minutes of stirring. Simultaneously, an equimolar amount (0.6756 g) of tetramethylammonium chloride (>98%, Aladdin) is dissolved in deionized water (4 mL), leading to solution B after 30 minutes of stirring. The two solutions, A and B, are then mixed and stirred thoroughly to obtain a clear and transparent yellow solution. At 70°C, a rapid solution evaporation process was employed for 5 hours to obtain powder samples for powder X-ray diffraction (XRD) testing. If the solution is allowed to stand for approximately 10 days, yellow crystals will precipitate from the solution, which is $[(\text{CH}_3)_4\text{N}][\text{FeCl}_4]$.

Then, plastic crystal films were fabricated. 5 mg plastic crystal was heated to 150 °C and maintained at the temperature for 10 minutes. Subsequently, a pressure (4 MPa, 6 MPa, 7 MPa, 8 MPa, or 16 MPa) was applied and maintained for 20 minutes. After the pressure was released, a dense $[(\text{CH}_3)_4\text{N}][\text{FeCl}_4]$ film was formed. Then the films were employed for thermal conductivity testing, differential scanning calorimetry (DSC), XRD, scanning electron microscopy (SEM), and infrared temperature testing. The basic information of the films is provided in Table S1.

The phase structures of the powders and films were analyzed using X-ray diffraction (XRD; 7000 S/L, Shimadzu Corp., Japan). Differential scanning calorimetry (DSC; Perkin Elmer Instruments, USA) was performed to determine the phase transition temperatures and heat capacity over a temperature range of 275-425 K, with

a heating rate of 5 K min⁻¹ in a nitrogen atmosphere. Scanning electron microscopy (SEM; Nova NanoSEM 450, Netherlands) was employed to observe the surface and cross-sectional morphology of the films. The temperature distribution of thin films can be measured by infrared temperature testing (FOTRIC, China).

Table S1: The basic information of the [(CH₃)₄N][FeCl₄] films

Pressure(MPa)	Thicknesses(μm)	Density(g/cm ³)
4	96	1.55
6	84	1.56
7	70	1.57
8	69	1.58
16	52	1.61

SM II. Details of measurements.

This study employed the 3-Omega method to measure the thermal conductivity of organic plastic crystal film [(CH₃)₄N][FeCl₄]. The traditional uniaxial heat conduction model of 3-Omega requires direct deposition of metal electrodes on the surface of the test film. However, due to the flexibility of organic films, depositing nano-electrodes on their surface can cause electrode deformation or even fracture. Therefore, for organic films, a bidirectional asymmetric heat conduction model is typically used, and the formula is shown as Equation S1[1, 2]. In this model, metal electrodes are first deposited on the substrate surface, and then the test film is bonded to the electrodes to protect the metal electrodes. For anisotropic films, the frequency-temperature rise

signal from a single metal electrode cannot provide the thermal conductivity in both the in-plane and cross-plane directions. This is because when the electrode width is much larger than the film thickness, the electrode is only sensitive to the cross-plane thermal conductivity. However, when the electrode width is comparable to or smaller than the film thickness, the electrode becomes sensitive to both in-plane and cross-plane thermal conductivities. Therefore, by using two metal electrodes with different widths, the in-plane and cross-plane thermal conductivities of the test film can be obtained[3].

The thickness of the plastic crystal films prepared in this experiment ranges from 40 to 100 μm . Considering the accuracy of signal measurements, the width of the metal electrodes in the 3-Omega method should not be too large. Therefore, the width of the metal electrodes in this experiment is all below 200 μm . Consequently, the electrodes are sensitive to the thermal conductivity in both directions [4]. First, the experiment needs to select a certain frequency interval to ensure that the thermal penetration depth can penetrate the film to be measured, and then measure the $V_{3\text{-}\omega}$ signal at different frequencies, as shown in Figure S1.

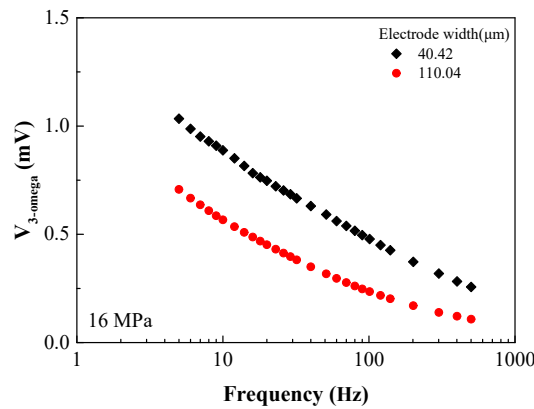


Figure S1: $V_{3\text{-}\omega}$ in relation to frequency

After obtaining the relationship between $V_{3-\omega}$ and frequency, the thermal conductivity is obtained by fitting the theoretical temperature rise with the experimental temperature rise using the least squares method. For a single electrode, both the thermal conductivity in the cross-plane direction and the anisotropy ratio are unknowns. According to Equation S1, by providing a series of anisotropy ratios (η), the corresponding thermal conductivity in the cross-plane direction (κ_{cross}) can be obtained. Then, by using the experimental signals from two electrodes of different widths, a set of relationships between κ_{cross} and η can be obtained. Since the κ_{cross} and η of the test film are constant, the intersection point of the curves represents the true κ_{cross} and η of the film.

$$\Delta T = \frac{P}{2\pi l} \int_0^\infty \frac{1}{\gamma_j} \frac{(A^+ + A^-)(B^+ + B^-) \sin^2(\lambda b)}{A^+ B^- - A^- B^+} \frac{d\lambda}{(\lambda b)^2} \quad (S1)$$

$$\gamma_j = \kappa_{cross, i} \sqrt{\eta_i \lambda^2 + \frac{2i\omega}{\alpha_{cross, i}}} \quad (S2)$$

Here, P , l and b represent the heating power, length, and half-width of the metal electrode, respectively; A^+ , A^- , B^+ and B^- are dimensionless parameters obtained by solving equations using the recursive matrix method; λ is the integration variable; $\kappa_{cross, i}$ and $\alpha_{cross, i}$ are the thermal conductivity and thermal diffusivity in the cross-plane direction of the i th layer, respectively.

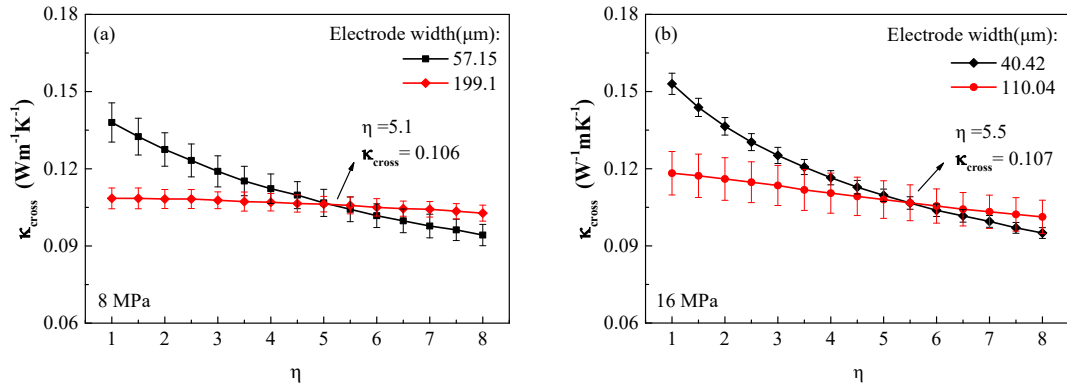


Figure S2: Thermal conductivity fitting results of the plastic crystal film: (a) 8 MPa; (b) 16 MPa.

SM III. Details of the EMD simulation.

In this work, the equilibrium method of molecular dynamics (EMD) was used to calculate the thermal conductivity, and all the simulation details are given in Table S1. The Green-Kubo formula is a result of linear response theory and the fluctuation dissipation theorem, which relates the heat flow autocorrelation to the thermal conductivity. k_B is the Boltzmann constant, V is the volume of the system, T is the temperature, τ is the relaxation time, τ_0 is the heat flux upper limit of the autocorrelation function, E is the kinetic energy of all atoms in the system, N is the number of atoms, and angular bracket is the system average. All molecular dynamics simulations in this paper are performed using the LAMMPS software package. The interatomic forces are taken from the universal force field [5] and the bond angles are taken from consistent valence force field [6]. The relevant parameters are listed in Table S2. This represents a challenging aspect of the simulation because the force fields are not specially developed for $[(CH_3)_4N][FeCl_4]$. In the simulations, the structure cannot keep a perfect crystal structure of $[(CH_3)_4N][FeCl_4]$, which takes error in the calculations. It may

minimize the error by specially developing a force field for $[(\text{CH}_3)_4\text{N}][\text{FeCl}_4]$ [7].

The long-range Coulombic force is calculated using the particle-particle particle-mesh (PPPM) method with an error parameter of 10^{-5} . Periodic boundary conditions are applied in all three dimensions. And the velocity verlet algorithm is employed to integrate equations of motion. 0.25 fs and 10 Å are chosen as time step and cutoff distance for the Lennard-Jones interaction, respectively. In addition, 8 independent simulations with different initial conditions are conducted to get better average. The simulation structures are simulated in NPT ensembles at target temperatures and 0 atm for 125 ps to obtain the optimized structures and simulation cell sizes, then followed by NVT ensembles for 125 ps before collecting heat flux of all six directions in NVE ensembles for 4 ns.

Table S1: Details of the simulation parameters.

Method			EMD (Green-Kubo method)		
Force field			Universal force field Consistent valence force field		
Boundary conditions			x y z: p p p		
Simulation process					
Ensemble	Setting				Purpose
NPT	Time step(fs)	0.25	Runtime(ns)	0.5	Relax structure
	Temperature(K)	330	Pressure(atm)	0	
NVT	Time step(fs)	0.25	Runtime(ns)	0.5	

	Temperature(K)	330	Thermostat	Nose- Hoover	
NVE	Sample interval time (fs)	3	Runtime(ns)	4	Data process
	Correlation time (ps)	25	Temperature(K)	330	
Recorded physical quantity					
Temperature			$\langle E \rangle = \sum_{i=1}^N \frac{1}{2} m_i v_i^2 = \frac{3}{2} N k_B T$		
Heat flux			$J = \frac{1}{V} \left[\sum_i e_i \vec{v}_i + \frac{1}{2} \sum_i \vec{r}_{ij} (\vec{F}_{ij} \cdot \vec{v}_i) \right]$		
Thermal conductivity			$\kappa = \frac{V}{3k_B T^2} \int_{\tau}^{\tau_0} \langle \vec{J}(0) \cdot \vec{J}(\tau) \rangle d\tau$		

Table S2: Parameter of force field

Atom type	Charge(e)	ϵ (kcal/mol)	$\sigma(\text{\AA})$
C	0.2481	0.105	3.851
Fe	3	0.013	2.912
Cl	-1	0.227	3.95
N	-0.6284	0.069	3.66
H	0.053	0.044	2.886

SM IV. Details of the relationship between thermal conductivity and the (002) crystal plane.

To investigate the relationship between the (002) crystal plane and thermal conductivity, it is calculated that the ratio (R_{XRD}) between this the integrated intensities of planes parallel to (002) and the sum of integrated intensities related to the other planes. The values of R_{XRD} and the ratio of thermal conductivity (R_{κ}) between the value along in-plane direction and cross-plane direction are plotted in Figure S3. It can be observed that the trend of R_{XRD} and R_{κ} with the pressure are similar, supporting that the preferential orientation of crystals influences thermal conductivity.

Compared to films prepared at 8 MPa, there is a slight decrease in (002) peak intensity and obvious decrease in (102) in the 16 MPa sample. Moreover, the XRD pattern for the 16 MPa film shows only three distinct peaks, indicating a closer resemblance to a single-crystal state. This could due to the formation of nearly single-crystal structure under higher pressure, which is shown in cross-sectional SEM images.

Combined with MD simulation results, it is evident that perfect plastically crystalline structures exhibit higher thermal conductivity along the (002) and (020) plane. Therefore, despite the slight decrease in (002) peak intensity for films prepared at 16 MPa, the formation of a more prominent, nearly single-crystal structure enhances their in-plane thermal conductivity.

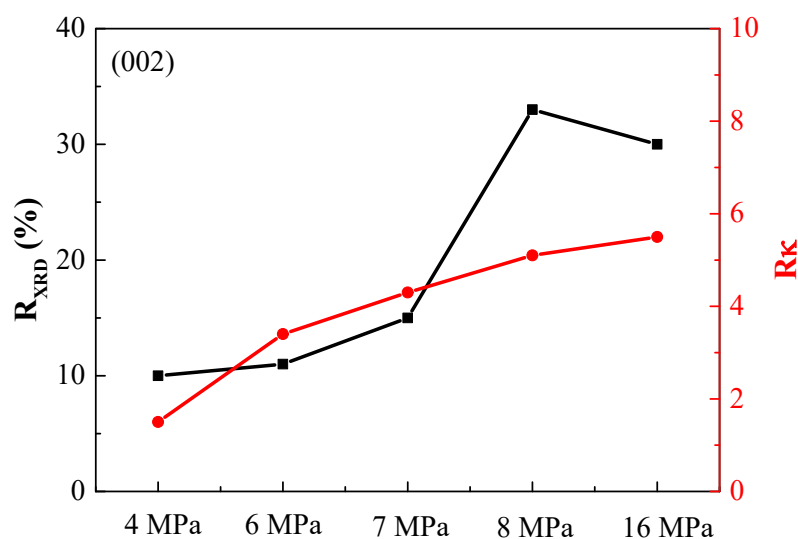


Figure S3. The values of R_{XRD} of (002) and R_k of films under different pressure.

SM V. Analysis of the Effects of Density and Porosity on the Thermal Conductivity of Plastic Crystals

As for the impact of density, quantitative measurements reveal that the density of the PCs film is changed 4% within the pressure range from 4 to 16 MPa, as shown in Table S1. This can be attributed to the inherent plasticity of $[(CH_3)_4N][FeCl_4]$, which, under uniaxial pressure, causes the crystal to elongate along other directions, resulting in small changes in density. Therefore, density has minimal impact on the thermal conductivity of the PCs film in this study.

Furthermore, the change of porosity is also not large because it is related to the density. There are many grain boundaries in porous structures, which cannot introduce anisotropy in thermal conductivity. As the increase of pressing, the porous structures and the number of boundaries is diminishing and the increasing crystal structures take

the anisotropy. Then, the phonon mean free path of crystal structures should be much larger than that of porous structures.

The anisotropic thermal conductivity of the PCs material studied here is primarily influenced by the microstructure and orientation of crystal structures.

From the SEM cross-sectional image (Figure 4) and XRD data (Figure 2(d)), it is evident that the film pressed at 4 MPa exhibits an unordered polycrystalline structure with disordered porous crystals. As the pressure increases, large layered grains gradually form within the film, and the intensity of the (002) crystal plane peak increases. Under 8 MPa hot-pressing, a clear formation of large layered grains is observed in the upper half of film samples.

Under 16 MPa hot-pressing, larger and more distinct single-crystal-like structures emerge within the film, forming pronounced layered structures, as shown in Figure 4(d) of the main text. Its XRD pattern shows only three main peaks: (002), (111), and (020), with other peaks either disappearing or weakening, also indicating that the film approaches a single-crystal state.

Additionally, MD simulation results (Figure 5) show that a perfect single-crystal structure exhibits significant thermal conductivity anisotropy, with the highest thermal conductivity along the [100] and [010] directions (parallel to the (002) crystal plane). Therefore, as the pressure increases, the crystals preferentially orient along the (002) plane, forming more complete layered structures that approach a single-crystal state, leading to an increase in the in-plane thermal conductivity and a significant thermal conductivity anisotropy in the film.

References

- [1] Feldman, A., High Temp-High Press 1999(31): p. 293.
- [2] Tong, T. and A. Majumdar, *Reexamining the 3-omega technique for thin film thermal characterization*. Review of Scientific Instruments, 2006. **77**(10).
- [3] Borca-Tasciuc, T., A.R. Kumar, and G. Chen, *Data reduction in 3 ω method for thin-film thermal conductivity determination*. Review of Scientific Instruments, 2001. **72**(4): p. 2139-2147.
- [4] Yamaguchi, S., T. Shiga, S. Ishioka, et al., *Anisotropic thermal conductivity measurement of organic thin film with bidirectional 3 ω method*. Review of Scientific Instruments, 2021. **92**(3).
- [5] Rappe, A.K., C.J. Casewit, K.S. Colwell, et al., *UFF, a full periodic table force field for molecular mechanics and molecular dynamics simulations*. Journal of the American Chemical Society, 1992. **114**(25): p. 10024-10035.
- [6] Dauber-Osguthorpe, P., Roberts V.A., Osguthorpe D.J., et al., *Structure and energetics of ligand binding to proteins: Escherichia coli dihydrofolate reductase-trimethoprim, a drug-receptor system*. Proteins: Structure, Function, and Bioinformatics, 1988. **4**(1): p. 31-47.
- [7] Qin Y., Zong Z., Che J., Li T., Fang H., Yang N., *Unveiling the thermal transport mechanism in compressed plastic crystals assisted by deep potential*. . arXiv:2501.12078, 2025.